Cancer vaccine attenuates carcinogen induced head and neck cancer with impaired early T cell response

Michihisa Kono[1,2], Masahiro Rokugo[1], John Quadarella[1], Shin Saito[1], Hiroki Komatsuda[1], Cong Fu[1], Sook-Bin Woo[3], Ann Marie Egloff[1,4], and Ravindra Uppaluri[1,4]*

[1]Department of Medical Oncology, Dana-Farber Cancer Institute, Boston, MA, USA,
[2]Department of Otolaryngology – Head and Neck Surgery, Asahikawa Medical University, Asahikawa, Japan,
[3]Division of Oral Medicine and Dentistry, Dana-Farber Cancer Institute and Brigham & Women's Hospital, Boston, Massachusetts,
[4]Department of Surgery/Otolaryngology, Brigham and Women's Hospital, Boston, MA, USA.

Email addresses

Michihisa Kono: Michihisa_Kono@DFCI.HARVARD.EDU

Masahiro Rokugo: Masahiro_Rokugo@DFCI.HARVARD.EDU

John Quadarella: John_Quadarella@dfci.harvard.edu

Shin Saito: SHIN_SAITO@DFCI.HARVARD.EDU

Hiroki Komatsuda: hiroki_komatsuda@dfci.harvard.edu

Cong Fu: Cong_Fu@DFCI.HARVARD.EDU

Sook-Bin Woo: swoo@bwh.harvard.edu

Ann Marie Egloff: aegloff@bwh.harvard.edu

Ravindra Uppaluri: RAVINDRA_UPPALURI@DFCI.HARVARD.EDU

***Corresponding author**

Ravindra Uppaluri, RAVINDRA_UPPALURI@DFCI.HARVARD.EDU

Keywords:

Head and neck cancer

4NQO carcinogenesis

Genetically engineered mouse model

Antigen-specific T cell

Impaired T cell response

DECLARATIONS

Ethics approval

All experimental animal procedures were approved by the institutional animal care and use committee (IACUC) of the Dana-Farber Cancer Institute.

Competing interests:

R.U. reports grants and personal fees from Merck, Regeneron and Daichi-Sankyo. The MOC models developed by R.U. have been filed with the Washington University Office of Technology Management and are licensed for distribution by Kerafast.

Funding

Work in Uppaluri lab is supported by NIH/NCI/NIDCR U01DE029188 and NIH/NIDCR R01DE027736.

Author contributions

Conceptualization, M.K. and R.U.; Methodology, M.K., A.M.E., and R.U.; Investigation, M.K., M.R., J.Q., S.S., H.K., and S.B.W.; Writing – Original Draft, M.K. and R.U.; Writing –Review & Editing, All authors; Funding Acquisition, R.U.; Resources, A.M.E. and R.U.; Supervision, A.M.E., and R.U.

Acknowledgements

We thank Dr. David Denardo for providing the OG mouse and Dr. Clint Allen for supplying reagents. We thank the NIH tetramer core for provision of reagents and all members of the Uppaluri lab for discussions.

ABSTRACT

Effective T cell immunotherapy requires understanding antigen-specific T cell development during tumorigenesis and immune surveillance. Here, we aimed to examine the dynamics of antigen-specific T cells from tumor initiation through progression in a tobacco carcinogen mimetic, 4-nitroquinoline-1-oxide (4NQO)-induced head and neck carcinogenesis model utilizing genetically engineered $K5^{CreERT/+}/ROSA^{OVA\text{-}GFP}/p53^{fl/fl}$ (KOG) mice. Our findings showed that early ovalbumin (OVA) expression via direct lingual tamoxifen (T) did not impact cancer development and survival, by comparing mice with tongue epithelium expressing OVA ($KOG/T/OVA^{+}$) to those without OVA ($KOG/T/OVA^{-}$) controlled by doxycycline. This equivalent tumor growth cannot be attributed to the loss of OVA expression. Intriguingly, although OVA-specific T cells were initially generated in tumor-draining lymph nodes (TDLN), they became undetectable 3 weeks after tamoxifen injection. Moreover, therapeutic anti-PD-1 was unable to restore OVA-specific T cells in TDLN and did not yield anti-tumor activity. Remarkably, OVA synthetic long peptide (SLP) vaccine induced OVA-specific T cells in KOG/T/OVA+ mice, and the combination of SLP vaccine and anti-PD-1 significantly reduced tongue tumor burden and prolonged survival. This study highlights the role of impaired endogenous antigen-specific T cell responses in immune resistance in head and neck cancer and the potential of cancer vaccines to improve outcomes.

97 **BACKGROUND**

98 Head and neck squamous cell carcinoma (HNSCC) represents the seventh most common cancer
99 worldwide, with 890,000 new cases diagnosed and 450,000 deaths each year (1). Patients with
100 human papillomavirus (HPV)-unrelated HNSCC, mainly caused by carcinogen exposure such as
101 tobacco, continue to suffer from recurrences or metastases, resulting in poor outcomes (1). These
102 cancers develop from pre-malignant dysplastic lesions progressing to invasive cancer in the
103 mucosal lining of the head and neck. Although not an immune desert malignancy, immune
104 checkpoint inhibitors (ICIs) that have been approved as first-line therapy for unresectable recurrent
105 or metastatic HNSCC show modest response rates (2). Thus, a better understanding of head and
106 neck cancer specific immune evasion mechanisms, including those occurring in pre-malignancy is
107 urgently needed.

108

109 Dissection of anti-tumor immune responses has revealed numerous mechanisms contributing to
110 immune resistance as codified in the cancer immunoediting hypothesis (3). HNSCCs have been
111 shown to exhibit several immune evasion mechanisms some of which include 1. down regulation
112 of tumor cell stimulator of interferon genes (STING) expression (4), 2. genomic alteration of
113 antigen processing machinery (5-7) and 3. a reduced adaptive T cell response possibly due to
114 immunosuppressive cellular influence (8, 9) and/ or dendritic cell dysfunction (10). The cancer
115 immunoediting hypothesis posits that tumor recognition and elimination occur at the earliest stages
116 of tumorigenesis, but the initial dynamics between oral neoplastic cells and antigen-specific T cells
117 leading to immune evasion are poorly understood. A major limitation has been the inability to
118 model interactions that retain the carcinogenic origin of these cancers while simultaneously
119 dissecting antigen-specific responses.

120

121 Herein, we established a model of 4-nitroquinoline-1-oxide (4NQO) carcinogen driven HNSCC
122 by administering the carcinogen to genetically engineered mice with tongue epithelium specific
123 Ovalbumin(OVA) expression and Tp53 gene deletion. Through this model, we aimed to
124 investigate how antigen expression impacts the progression from oral premalignancy to invasive
125 HNSCC, focusing on the dynamics of antigen-specific T cells dynamics.

126

127

128 **MATERIALS AND METHODS**

129 **Sex as a biological variant**

130 Our study examined male and female animals, and similar findings are reported for both sexes.

131

132 **Mouse models**

133 $Rosa^{OVA\text{-}GFP(OG)}/Tp53^{f/f}$ mice have been described and were obtained from Dr. David Denardo (11)
134 and $K5^{Cre\text{-}ERT/+}$/ mice were obtained from the Jackson Laboratory. Mice were bred to obtain $K5^{Cre\text{-}}$
135 $^{ERT/+}$/ $Rosa^{OVA\text{-}GFP(OG)}/Tp53^{f/f}$ (KOG) on the C57BL/6J background. The OG cassette was bred to
136 homozygosity. All experiments used 6–10-week-old, male and female mice and experimental
137 groups were matched in age and the number of males and females. TCR-transgenic OT-1 mice
138 (C57BL/6-Tg (TcraTcrb)1100Mjb) were purchased from the Jackson Laboratory and bred in-
139 house. All mice were maintained under pathogen-free conditions, and all animal experiments were
140 approved by the institutional animal care and use committee (IACUC) at the Dana-Farber Cancer
141 Institute.

142

143 **Administration of 4NQO, doxycycline and tamoxifen**

144 4NQO (Sigma Aldrich) was dissolved in DMSO at a concentration of 50 mg/mL and then diluted
145 in sterile water to a final concentration of 100µg/mL. KOG mice were exposed to 4NQO in their
146 drinking water for 8 weeks and then switched to normal drinking water. (12). 4NQO drinking
147 water was used in disposable cages and replaced weekly. In some experiments, doxycycline (625
148 mg/kg) was administered at the same time as the 4NQO drinking water. Fort he tamoxifen
149 injections, we used the injection methodology described by Carper et al(13). A total of 30µl of
150 1mM 4-OHT (4-Hydroxytamoxifen, Selleck) in corn oil was injected into the epithelium of the
151 tongue 3 times every 2 days on day 3, 5, 7 after 4NQO and doxycycline administration began.
152 Following exposure to 4NQO, mice were visually checked for tumor development and weighed at
153 least weekly.

154

155 **Tissue harvest**

156 The KOG mice were sacrificed for humane endpoints decided by IACUC guidelines. Harvested
157 lymph nodes (LNs) and spleen were processed into single cell suspensions using microscope slide
158 glasses. Harvested tongues and tumors were dissociated using razor blades and then incubated with
159 RPMI (Life Technologies) with collagenase Type IV (100µg/ml, Life Technologies) for 30 min at
160 37°C. Tongues were fixed in 10% formalin for 24 h. Following fixation, the long-axis of tongues
161 were sectioned along the long axis and embedded in paraffin.

162

163 **Macroscopic tumor measurement**

164 Tumor-bearing mice were photographed under anesthesia by retracting the tongue anteriorly and
165 capturing images of the dorsum. ImageJ software was used to measure the area of the tongue and

166 tumor, and the percentage of tumor area to tongue was calculated. The number of tumors per
167 tongue were also counted.
168
169 **Microscopic evaluation**
170 FFPE sections were stained with hematoxylin and eosin (H&E) and histopathological evaluation
171 was performed by a board certified oral pathologist (S.B.W.). The evaluating pathologist was
172 blinded to the treatment arms. The epithelial hyperplasia score was categorized into four levels (0-
173 3). Meanwhile, the histopathological scoring of the most severe lesion was stratified into six levels:
174 0 for Normal, 1 for Atypia, 2 for Mild Dysplasia, 3 for Moderate Dysplasia, 4 for Severe Dysplasia
175 or Severe Papillary Dysplasia, and 5 for Squamous Cell Carcinoma (SCC).
176
177 **Establishment of organoids**
178 The methods for organoid culture and the medium formulation were adapted from Karakasheva et
179 al.(14) with specific modifications for our study needs. Tongues from KOG mice were harvested,
180 and then the epithelium was isolated using scissors and a dissecting microscope. Tongue
181 epitheliums were incubated in HBSS (Thermo Fisher Scientific) with dispase (1:5, Corning),
182 Fungizone (1:500, Thermo Fisher Scientific), gentamycin (1:10000, Thermo Fisher Scientific),
183 and penicillin streptomycin (1:1000, Thermo Fisher Scientific) for 30min at 37°C in a thermomixer
184 (700-800RPM). Tissues were removed from HBSS, incubated with 0.25% trypsin EDTA (Life
185 Technologies) for 10 minutes, filtered through a strainer with soybean trypsin inhibitor (Sigma-
186 Aldrich) and centrifuged. A similar procedure was used to make tumors organoids. Single cells
187 (2000) were resuspended in 30µl Matrigel Matrix (Corning) with organoid media (1:1) and
188 droplets were plated in a pre-warmed 24 well plate (Thermo Fisher Scientific). After incubation

189 of the droplets at 37°C for 15min, pre-warmed organoid media was added. Organoid media was
190 constituted of advanced DMEM/F12 (Thermo Fisher Scientific) with WRN conditioned media
191 (3:100 Wnt/Noggin/R-Spondin), penicillin streptomycin (1:100, Thermo Fisher Scientific),
192 HEPES (1:100, Life Technologies), Glutamax (1:100, Life Technologies), Gibco B-27
193 Supplement (2:100, Life Technologies), Gibco N-2 Supplement (1:100, Life Technologies), N-
194 Acetylcysteine (0.5M, 2:1000, Fisher Scientific), mEGF (500µg/ml, 1:20000, Life Technologies)
195

196 **Flow cytometry**

197 Isolated cells were stained with 1:500 Zombie Aqua (BioLegend) in PBS for 15 min at room
198 temperature (RT). For SIINFEKL-tetramer staining, washed cells were incubated with 1:1000 PE-
199 conjugated SIINFEKL tetramer (NIH tetramer core) in PBS with 0.5% FBS and 2 mM EDTA for
200 15 min at RT. For HAAHAEINEA-tetramer staining, cells were incubated with 1:100 PE-
201 conjugated HAAHAEINEA tetramer (NIH tetramer core) in PBS with 0.5% FBS and 2 mM EDTA
202 for 60 min at 37°C. Cells were then resuspended Fc block (BioLegend) for 10 min at 4°C and
203 stained with 1:200 anti-mouse antibodies (Abs) in PBS with 0.5% FBS and 2 mM EDTA for 20
204 min at 4°C. For organoid assessment, organoids were pretreated with 2.5 mM 4-OHT for 96h and
205 then with 2 µg/mL doxycycline for 48 h. For H2kb-SIINFEKL staining, cells were pretreated with
206 100 U/mL IFN-γ for 24h and stained with 1:1000 H2kb-SIINFEKL Ab (BioLegend,Clone:25-
207 D1.16). GFP-expressing cell lines were used for GFP compensation. Data were acquired on
208 Miltenyi MACSQuantX flow cytometer and analyzed using FlowJo v10.8.1 (BD) software.
209

210 **ELISA**

211 T cells from KOG mouse TDLNs (5×10^5) were co-cultured with SIINFEKL peptide (1 μg/mL,
212 Thermo Fisher Scientific) in a 96-well plate (Thermo Fisher Scientific). For the *in vitro* OT-1 co-
213 culture assay, tumor cells ($5x10^4$) were co-cultured with T cells ($5x10^5$) from OT-1 mouse
214 splenocytes. After 24h, the supernatant was measured by IFN-γ ELISA (R&D) following
215 manufacturer's instructions.
216
217 **Adoptive OT-1 cell transfer**
218 CD8+ T cells from OT-1 mouse splenocytes were purified with CD8a+ isolation kit, mouse
219 (Miltenyi Biotec) and then labeled with Carboxyfluorescein Succinimidyl Ester (CFSE) using
220 CFSE Cell Division Tracker Kit (BioLegend) according to manufacturer's instructions. OT-1
221 CD8+ T cells (5×10^5) were retro-orbitally injected into tumor-bearing KOG mice. LNs were
222 harvested on day 3 after transfer and the CFSE-labeled CD8+ OT-1 T cells were assessed by flow
223 cytometry. CFSE-positive cells were divided into CFSE-high (before or during proliferation) and
224 -low cells (post-activation and proliferation) and their percentages were compared.
225
226 **Vaccination**
227 For peptide vaccine treatment, OVA-derived synthetic long peptide (SLP, 50 μg,
228 SMLVLLPDEVSGLEQISIINFEKLTEWTS, Peptide2.0) was injected into buccal mucosa of
229 tumor-bearing KOG mice 3 times every 3 days along with 100 μg polyI:C (Invitrogen) as adjuvant.
230
231 **Cell lines and inoculation**
232 The mouse oral squamous cell carcinoma MOC1 was generated as previously described (15) (16)
233 (17). The mKate2-SIINFEKL plasmid was kindly provided by Dr. Clint T. Allen (National

234 Institutes of Health) and SIINFEKL-expressing MOC1 (MOC1OVA) was engineered as
235 previously described (18) (10) . These cell lines were tested for mycoplasma every 6 months. All
236 cell lines were cultured with the 2:1 mixture of IMDM (Life technologies) and Ham's-F12 nutrient
237 mixture (Thermo Fisher Scientific) with 100 U/mL penicillin streptomycin (Thermo Fisher
238 Scientific), 5% heat inactivated Fetal Bovine Serum (FBS) (Sigma Aldrich), 5 ng/mL Epidermal
239 Growth Factor (EGF) (Life Technologies), 400 ng/mL hydrocortisone (Sigma Aldrich), and 5
240 μg/ml insulin (Sigma Aldrich). 3×10^6 MOC1 cells were inoculated into the buccal mucosa of KOG
241 mice or wildtype C57BL/6 mice.
242
243 **In vivo antibody treatment**
244 Anti-PD-1 mAb (250 μg, clone: RMP1-14, BioXCell) or isotype control (BioXCell) was injected
245 intraperitoneally into KOG mice. Anti-CD40L Ab (BioXCell, 250μg) was injected
246 intraperitoneally on day 14.
247
248 **Statistical analysis**
249 Statistical analyses were carried out using GraphPad Prism 9 software (GraphPad). Comparisons
250 of two independent groups were performed using Student's *t*-test and multiple comparisons were
251 evaluated using ANOVA with Tukey's multiple comparison adjustment. Kaplan–Meier curves
252 and log rank tests were used to assess survival differences. Differences were considered
253 statistically significant at two-sided $p < 0.05$, marked as $*p < .05$, $**p < .01$, $***p < .001$, and ns =
254 not significant. All data are shown as means ±SEM.
255
256

257 **RESULTS**

258 **Establishment of a HNSCC mouse model with tongue epithelium-specific OVA expression**
259 **and p53 deletion**

260 The development of a chemically induced HNSCC model using 4NQO, a carcinogen that induces
261 tobacco-associated gene mutation signatures, poses significant challenges for tracking antigen-
262 specific T cells due to tumor heterogeneity. To address these challenges, we developed a 4NQO-
263 induced oral cancer model using genetically engineered $K5^{Cre\text{-}ERT/+}$; $Rosa^{OVA\text{-}GFP(OG)}$; $p53^{f/f}$ (KOG)
264 mice. The OG mice, previously utilized in pancreatic and lung cancer models (11) were engineered
265 to enable tongue epithelial basal keratinocyte keratin 5 (K5)-specific expression of OVA antigen
266 and knockout of p53 upon tamoxifen injection (Figure 1A). Antigen expression is turned off with
267 doxycycline administration. By administering 4NQO to these mice, we established an HNSCC
268 mouse model that closely mimics human HNSCC with specific antigen expression, as shown in
269 Figure 1A.

270 To validate this genetic strategy, we first created organoids from the normal epithelium of $K5^{Cre\text{-}}$
271 $^{ERT/+}$; $Rosa^{OG/+}$; $p53^{f/+}$ mice (Figure 1B). Organoids derived from normal tongue epithelium
272 increased GFP and H2-K^b-SIINFEKL expression upon tamoxifen treatment, and expression was
273 abolished with doxycycline treatment (Figure 1C and D). Next, to confirm that this genetic
274 modification works in vivo, tamoxifen was injected into the KOG mouse tongues 3 times every 2
275 days in the presence or absence of doxycycline. One week later, the tongues were harvested and
276 single cells were analyzed by flow cytometry (Figure 1E). Results confirmed that GFP and H2-
277 K^b-SIINFEKL were also expressed by tamoxifen injection in vivo and eliminated by doxycycline
278 feeding (Figure 1F and G). Together, we established a novel genetically engineered mouse with
279 regulatable expression of tongue epithelium-specific OVA antigen .

280

281 **Early expression of OVA antigen did not affect 4NQO-induced HNSCC progression**

282 Using the KOG mouse, we investigated how early antigen load affects carcinogen-induced
283 tumorigenesis and anti-tumor immunity (Figure 2A). Mice were treated with 4NQO water for 8
284 weeks and then switched to normal water (Figure 2A). Lingual tamoxifen injection (T) to induce
285 OVA expression and delete Tp53 was performed 3 days after the start of 4NQO water treatment
286 (KOG/T/OVA$^+$). A matched cohort was concurrently fed a doxycycline diet to turn off OVA
287 expression (KOG/T/OVA$^-$). Surprisingly, the tongues of KOG/T/OVA$^+$ formed atypia and mild
288 dysplasia at 9-15 weeks, and progressed to severe dysplasia and carcinoma at 23-30 weeks,
289 comparable to KOG/T/OVA$^-$ mice without elimination of antigen response (Figure 2B-D). At 22
290 weeks, macroscopic tumor area and number of tumors per mouse were determined to be
291 comparable in both groups (Figure 2E, F, and S1). Similarly, overall survival rates and mouse
292 weights showed no significant differences (Figures 2G and H). These results indicated that early
293 expression of OVA antigen during tumorigenesis did not significantly affect tumor development
294 in this model.

295

296 **OVA antigen is maintained on tumor cells during tumorigenesis**

297 To determine whether the loss of OVA expression was responsible for the equivalent tumor growth
298 in the comparative experiment, we first assessed GFP expression in tongue epithelium of
299 KOG/T/OVA$^+$ at 12-weeks and observed no loss of GFP fluorescence (Figure 3A). Second,
300 organoids were created from 25-week-old KOG/T/OVA$^+$ mice and we found that these cells
301 continued to express GFP and also H2-K^b-SIINFEKL (Figure 3B, C, and S2A). Third, confirming
302 that tumor cells were recognized by OVA-specific T cells, OT-1 CD8+ T cell co-culture

303 supernatants were positive for IFN-γ, indicating antigen specific OT-1 CD8 T cell activation
304 (Figure 3D). Finally, we then examined whether antigen was processed and presented in tumor-
305 draining lymph nodes (TDLNs). CFSE-labeled OT-1 $CD8^+$ T cells were transferred into tumor-
306 bearing KOG/T/OVA^+ mice (20 weeks post-4NQO) and TDLNs were harvested 3 days after
307 transfer (Figure 3E). OT-1 CD8+ T cells responded to antigen and proliferated in TDLNs (Figure
308 3F, G, and S2B). From these results, we concluded that OVA expression was maintained during
309 4NQO-induced tumor development in mice without doxycycline.
310
311 **OVA-specific T cells were generated but subsequently became undetectable**
312 Given that OVA antigen expression was maintained in the tongue epithelium and in tumor tissue
313 during tumor progression, we hypothesized that the underlying cause of the lack of tumor
314 regression by anti-tumor immunity was dysfunction within the T cell compartment. Thus, we
315 chronologically assessed OVA-specific T cells in TDLNs throughout the 4NQO carcinogenesis
316 protocol (Figure 4A). SIINFEKL-tetramer+ T cells were initially generated in TDLNs one week
317 after the last injection of tamoxifen but surprisingly became undetectable three weeks later and
318 remained absent through the remainder of observation and endpoint of study (Figure 4B, C, and
319 S3A). Supernatants of TDLN cultures with SIINFEKL peptide were assayed by IFN-γ ELISA, and
320 OVA-reactive T cells were initially detected ex vivo but no OVA-reactive T cells were detected
321 by the 4-week timepoint (Figure 4D). OVA-specific CD4 T cells, which are not regulatory T cells,
322 were also generated early on but were not detected later (Figure S3B). OVA-specific T cells
323 remained lost even after the stimulation with a CD40 agonist, which was administered when these
324 T cells were still present. (Figure S3C). To determine whether KOG mice have immune tolerance
325 to OVA, we transplanted an OVA-expressing syngeneic mouse oral carcinoma (MOC1-OVA) into

326 the buccal mucosa of KOG or wildtype C57BL/6 mice (Figure 4E). OVA-specific T cells were
327 generated in KOG mouse tumors and TDLNs but their numbers were reduced compared to
328 wildtype C57BL/6 mice (Figure 4F and G). These results suggest that KOG mice retain the cellular
329 capacity to react to OVA antigen albeit at a reduced level compared to wild type mice and that
330 tamoxifen-induced OVA-specific T cells became subsequently undetectable. Collectively, these
331 data are consistent with impaired OVA-specific T cell response as the reason why antigen activated
332 T cell response did not reduce tumor growth.
333
334 **Anti-PD-1 blockade did not restore OVA-specific T cell responses nor anti-tumor efficacy**
335 We next examined the possible anti-tumor effects of anti-PD-1 blockade on 4NQO-induced KOG
336 tumors. Anti-PD-1 antibody was injected twice weekly into tumor-bearing mice with or without
337 OVA-expression (Figure 5A). Anti-PD-1 therapy did not result in tumor regression in either
338 KOG/T/OVA^{+} or KOG/T/OVA^{-} tumors (Figure 5B-D). Moreover, CD8+ T cells and PD-1+ CD8+
339 T cells were not increased by anti-PD-1 blockade (Figure 5E and F). SIINFEKL-tetramer+ T cells
340 were not detected in KOG/T/OVA^{+} tumors, even with anti-PD-1 blockade treatment. (Figure 5G).
341 To examine whether OVA-specific T cells were initially present in an anergic state due to the PD-
342 1 checkpoint, mice were treated with anti-PD-1 blockade at an earlier timepoint, when OVA-
343 specific T cells were not detectable (Figure 5H). In this setting, anti-PD-1 inhibition also did not
344 restore OVA-specific T cells (Figure 5I and J). These results suggested that KOG tumors were
345 resistant to anti-PD-1 treatment regardless of OVA expression and anti-PD-1 blockade did not
346 revive OVA-specific T cells.
347

348 **Peptide vaccine restores OVA-specific T cells and attenuates tumor growth in combination**
349 **with anti-PD-1**

350 As impaired OVA specific T cell response was identified as a potential mechanism of immune
351 evasion by OVA-expressing tumors in KOG mice, we next aimed to definitively examine if tumor
352 control could be achieved with antigen specific T cells. Given the observed T cell response to
353 MOC1-OVA, we tested whether OVA-specific T cells could be generated by OVA synthetic long
354 peptide (SLP) and PolyI:C vaccine. Tumor-bearing mice were vaccinated with 3 doses of an OVA
355 SLP in the buccal mucosa (Figure 6A). As shown in Figure 6B and C, this vaccine induced OVA-
356 tetramer+ T cells in both KOG/T/OVA^{+} and KOG/T/OVA^{-} oral draining lymph nodes. OVA
357 peptide co-culture and ELISA experiments confirmed that these T cells could recognize the OVA
358 peptide effectively (Figure 6D).

359 Finally, we evaluated the anti-tumor efficacy of the peptide vaccine combined with anti-PD-1
360 therapy (Figure 6E). Remarkably, OVA SLP peptide and polyI:C vaccine with anti-PD-1 Ab
361 significantly reduced the KOG tumor area compared to control group receiving PolyI:C plus anti-
362 PD-1 therapy (Figure 5F-H). Moreover, overall survival was prolonged by OVA vaccine treatment
363 (Figure 5I). Taken together, vaccination induced antigen-specific T cells in mice bearing oral
364 tumor with immune evasion mechanisms involving impaired endogenous antigen-specific T cell
365 response. This therapeutic approach resulted in tumor regression and extended survival.

366

367

368

369

370

371 **DISCUSSION**

372 The carcinogen 4NQO triggers tumor genetic mutations similar to those found in human tobacco-
373 related HNSCC (19) (20). Furthermore, 4NQO-induced malignancy also showed similar immune
374 infiltration and response rate to anti-PD-1 therapy similar to those observed in human HNSCC
375 (21). The advantage of the 4NQO model lies not only in its resemblance to human HNSCC, but
376 also in its capability to observe tumorigenesis from its earliest stages. While the mutational burden
377 is higher in invasive squamous cell carcinomas (SCCs) than hyperplasia and mild dysplasia, it is
378 crucial to note that critical mutations in genes such as p53, Notch1, and Fat1 can already be
379 detected in early-stage lesions (22). Recent studies of 4NQO-induced cancers at different
380 pathological stages have also demonstrated that key immune-related genes increase from the
381 dysplasia stage (23). In this study, we generated a 4NQO-induced HNSCC mouse model with
382 genetically engineered epithelium-specific OVA expression. This unique model allows for the
383 observation of immunoediting by endogenous antigen expression during tumorigenesis while
384 maintaining HNSCC heterogeneity.

385

386 Other spontaneous cancers models have explored how antigen induction impacts tumor
387 development, emphasizing its effect on eliciting tissue-specific immune responses. For example,
388 in KPC mouse lung cancers with KRAS(G12D) activating mutation, p53 knockout and bearing
389 the OG cassette, OVA expression led to tumor shrinkage (11). In contrast, in pancreatic cancer
390 expression of this same antigen resulted in enhanced tumor growth due to cDC deficiency (11).
391 Tissue-specific immune responses have been thoroughly investigated in the contexts of infectious
392 diseases and autoimmunity, and their relevance to tumor immunity has also been established.
393 These site specific responses also translate to ICI responses, as outcomes are markedly different

394 depending on the site of metastasis (24). In preclinical syngeneic models, orthotopic
395 transplantation has been shown to have a weaker immune surveillance relative to subcutaneous
396 inoculation (25). However, in contrast to this finding, we observed that orthotopic oral inoculation
397 elicits a stronger immune response and leads to tumor reduction compared to subcutaneous
398 inoculation, again highlighting the difference in tissue-specific immune responses depending on
399 cancer type and tumor site (26). To further understand HNSCC specific responses in the
400 autochthonous setting, we engineered a HNSCC-specific preclinical model bearing the OG
401 cassette. This approach aims to elucidate the role of the anti-tumor T cell immunity in HNSCC.
402
403 We observed that antigen-specific T cells were initially generated as a result of strong antigen
404 expression from the early tumorigenesis but were consequently undetectable in peripheral tissues.
405 With this absence of an antigen-specific response, we saw no difference in tumorigenesis
406 compared to the antigen-free tumors and a similar absence of anti-PD-1 therapeutic efficacy. T
407 cell absence is classified as central thymic tolerance during T cell development with subsequent
408 peripheral loss (27). In this model, central tolerance to OVA-specific T cells may have developed
409 presumably by leaky antigen expression in thymocytes. Leaky expression has been a known
410 problem with the conventional inducible antigen engineered models because low level self-antigen
411 expression can cause thymic tolerance (28, 29) (30). The recently described NINJA (inversion
412 inducible joined neoantigen) model aims to prevent leaky neoantigen expression and tolerance (31,
413 32).
414 Since neoantigens are not expressed in normal tissues and development, the T cell repertoire
415 maintains intact to mount anti-tumor responses to mutant allele products. Thus, our OG cassette-
416 derived antigen most closely resembles tumor-associated antigens (TAAs) rather than neoantigens.

417 Neoantigens have been extensively studied for their high immunogenicity but treatments utilizing
418 personalized neoantigen-specific T cells are limited in their application across a broad patient
419 population due to the unique tumor- and patient-specific characteristics. Thus, therapies targeting
420 shared antigens, including TAAs, have been a focus of many studies (33) (34) (35). Notably, a
421 detailed analysis of recent successful TIL therapy clinical trial in stage IV melanoma patients
422 revealed that responding tumor-specific T cells targeted shared TAA-specific T cells and not
423 neoantigen-specific T cells (36). This finding highlights the significance of researching TAA-
424 specific T cells for advancing cancer treatment strategies.
425
426 In this study, central tolerance did not eliminate all OVA-specific T cells, however, upon antigen
427 expression early in tumorigenesis, antigen-specific T cells were impaired in the periphery.
428 Peripheral tolerance, as well as central tolerance, is crucial for preventing autoimmunity immune.
429 Various mechanisms, both T cell intrinsic, such as anergy and clonal deletion, and T cell extrinsic,
430 such as regulatory T cells, contribute to peripheral T cell tolerance (27, 37) (38). For instance,
431 activated antigen-specific T cells in liver metastases were eliminated by $FasL^+$ monocyte-derived
432 macrophages, leading to acquired immunotherapy resistance (39). It is well recognized that
433 checkpoint receptors, such as PD-1, play a role in promoting peripheral tolerance by causing the
434 deletion or anergy of anti-tumor T cells (40, 41). Recent studies using the NINJA model revealed
435 that PD-1 molecules result in peripheral tolerance, allowing the coexistence of antigen-expressing
436 cells and antigen-specific T cells without an ongoing response (38). Our data that anti-PD-1
437 blockade did not restore antigen-specific T cells suggests that this mechanism was not occurring
438 in our model system.
439

440 Despite the lack of an ongoing CD8+ T cell response, the therapeutic relevance of continued
441 antigen expression in anti-PD-1 resistant tumors was highlighted by anti-tumor responses observed
442 following vaccination against OVA. We found that that antigen-specific T cells, which were
443 undetectable by tetramer and ex vivo peptide short stimulation, were induced by the vaccine,
444 leading to tumor regression. These results suggest defining target antigens independent of
445 endogenous antigen-specific T cell responses as a therapeutic strategy. Further investigation is
446 needed to explore the specific TCRs recognizing the endogenous OG cassette expression versus
447 those induced by vaccination. This study also supports the rationale for combining targeted
448 immunotherapies, like cancer vaccines, with non-specific immunotherapies, such as anti-PD-1
449 inhibitors, for immune-cold tumors due to antigen-specific T cell deletion. This approach aligns
450 with clinical evidence demonstrating the synergistic effects of combining cancer vaccines with
451 anti-PD-1 inhibitors (42), suggesting a promising approach for enhancing therapeutic efficacy
452 against these challenging tumor types including HNSCC. In conclusion, this study highlights a
453 strategy for targeting tumors that evade the immune surveillance through impaired early T cell
454 response in HNSCC.
455
456
457
458
459
460
461
462

463 **REFERENCES**
464

465 1. Ruffin AT, Li H, Vujanovic L, Zandberg DP, Ferris RL, and Bruno TC. Improving head
466 and neck cancer therapies by immunomodulation of the tumour microenvironment. *Nat*
467 *Rev Cancer.* 2023;23(3):173-88.
468 2. Gillison ML, Blumenschein G, Fayette J, Guigay J, Colevas AD, Licitra L, et al. Long-
469 term Outcomes with Nivolumab as First-line Treatment in Recurrent or Metastatic Head
470 and Neck Cancer: Subgroup Analysis of CheckMate 141. *Oncologist.* 2022;27(2):e194-
471 e8.
472 3. Schreiber RD, Old LJ, and Smyth MJ. Cancer immunoediting: integrating immunity's
473 roles in cancer suppression and promotion. *Science.* 2011;331(6024):1565-70.
474 4. Hayman TJ, Baro M, MacNeil T, Phoomak C, Aung TN, Cui W, et al. STING enhances
475 cell death through regulation of reactive oxygen species and DNA damage. *Nature*
476 *communications.* 2021;12(1):2327.
477 5. Comprehensive genomic characterization of head and neck squamous cell carcinomas.
478 *Nature.* 2015;517(7536):576-82.
479 6. Grandis JR, Falkner DM, Melhem MF, Gooding WE, Drenning SD, and Morel PA.
480 Human leukocyte antigen class I allelic and haplotype loss in squamous cell carcinoma of
481 the head and neck: clinical and immunogenetic consequences. *Clinical cancer research :*
482 *an official journal of the American Association for Cancer Research.* 2000;6(7):2794-
483 802.
484 7. López-Albaitero A, Nayak JV, Ogino T, Machandia A, Gooding W, DeLeo AB, et al.
485 Role of antigen-processing machinery in the in vitro resistance of squamous cell
486 carcinoma of the head and neck cells to recognition by CTL. *Journal of immunology.*
487 2006;176(6):3402-9.
488 8. Clavijo PE, Moore EC, Chen J, Davis RJ, Friedman J, Kim Y, et al. Resistance to CTLA-
489 4 checkpoint inhibition reversed through selective elimination of granulocytic myeloid
490 cells. *Oncotarget.* 2017;8(34):55804-20.
491 9. Sun L, Clavijo PE, Robbins Y, Patel P, Friedman J, Greene S, et al. Inhibiting myeloid-
492 derived suppressor cell trafficking enhances T cell immunotherapy. *JCI Insight.*
493 2019;4(7).
494 10. Saito S, Kono M, Nguyen HCB, Egloff AM, Messier C, Lizotte P, et al. Targeting
495 Dendritic Cell Dysfunction to Circumvent anti-PD1 Resistance in Head and Neck
496 Cancer. *Clin Cancer Res.* 2024.
497 11. Hegde S, Krisnawan VE, Herzog BH, Zuo C, Breden MA, Knolhoff BL, et al. Dendritic
498 Cell Paucity Leads to Dysfunctional Immune Surveillance in Pancreatic Cancer. *Cancer*
499 *Cell.* 2020;37(3):289-307.e9.
500 12. Wu JS, Zheng M, Zhang M, Pang X, Li L, Wang SS, et al. Promotes 4-Nitroquinoline-1-
501 Oxide-Induced Oral Carcinogenesis With an Alteration of Fatty Acid Metabolism. *Front*
502 *Microbiol.* 2018;9:2081.
503 13. Carper MB, Troutman S, Wagner BL, Byrd KM, Selitsky SR, Parag-Sharma K, et al. An
504 Immunocompetent Mouse Model of HPV16(+) Head and Neck Squamous Cell
505 Carcinoma. *Cell Rep.* 2019;29(6):1660-74.e7.
506 14. Karakasheva TA, Kijima T, Shimonosono M, Maekawa H, Sahu V, Gabre JT, et al.
507 Generation and Characterization of Patient-Derived Head and Neck, Oral, and
508 Esophageal Cancer Organoids. *Curr Protoc Stem Cell Biol.* 2020;53(1):e109.

509 15. Judd NP, Winkler AE, Murillo-Sauca O, Brotman JJ, Law JH, Lewis JS, Jr., et al.
510 ERK1/2 Regulation of CD44 Modulates Oral Cancer Aggressiveness. *Cancer research.*
511 2012;72(1):365-74.
512 16. Onken MD, Winkler AE, Kanchi KL, Chalivendra V, Law JH, Rickert CG, et al. A
513 surprising cross-species conservation in the genomic landscape of mouse and human oral
514 cancer identifies a transcriptional signature predicting metastatic disease. *Clinical cancer*
515 *research : an official journal of the American Association for Cancer Research.*
516 2014;20(11):2873-84.
517 17. Kono M, Saito S, Egloff AM, Allen CT, and Uppaluri R. The mouse oral carcinoma
518 (MOC) model: A 10-year retrospective on model development and head and neck cancer
519 investigations. *Oral oncology.* 2022;132:106012.
520 18. Sun L, Moore E, Berman R, Clavijo PE, Saleh A, Chen Z, et al. WEE1 kinase inhibition
521 reverses G2/M cell cycle checkpoint activation to sensitize cancer cells to
522 immunotherapy. *Oncoimmunology.* 2018;7(10):e1488359.
523 19. Bhatia S, Oweida A, Lennon S, Darragh LB, Milner D, Phan AV, et al. Inhibition of
524 EphB4-Ephrin-B2 Signaling Reprograms the Tumor Immune Microenvironment in Head
525 and Neck Cancers. *Cancer Res.* 2019;79(10):2722-35.
526 20. Cao Y, Dong H, Li G, Wei H, Xie C, Tuo Y, et al. Temporal and spatial characteristics of
527 tumor evolution in a mouse model of oral squamous cell carcinoma. *BMC Cancer.*
528 2022;22(1):1209.
529 21. Wang Z, Wu VH, Allevato MM, Gilardi M, He Y, Luis Callejas-Valera J, et al.
530 Syngeneic animal models of tobacco-associated oral cancer reveal the activity of in situ
531 anti-CTLA-4. *Nature communications.* 2019;10(1):5546.
532 22. Sequeira I, Rashid M, Tomás IM, Williams MJ, Graham TA, Adams DJ, et al. Genomic
533 landscape and clonal architecture of mouse oral squamous cell carcinomas dictate tumour
534 ecology. *Nat Commun.* 2020;11(1):5671.
535 23. Lee YM, Hsu CL, Chen YH, Ou DL, Hsu C, and Tan CT. Genomic and Transcriptomic
536 Landscape of an Oral Squamous Cell Carcinoma Mouse Model for Immunotherapy.
537 *Cancer Immunol Res.* 2023;11(11):1553-67.
538 24. Tumeh PC, Hellmann MD, Hamid O, Tsai KK, Loo KL, Gubens MA, et al. Liver
539 Metastasis and Treatment Outcome with Anti-PD-1 Monoclonal Antibody in Patients
540 with Melanoma and NSCLC. *Cancer Immunol Res.* 2017;5(5):417-24.
541 25. Horton BL, Morgan DM, Momin N, Zagorulya M, Torres-Mejia E, Bhandarkar V, et al.
542 Lack of CD8(+) T cell effector differentiation during priming mediates checkpoint
543 blockade resistance in non-small cell lung cancer. *Sci Immunol.* 2021;6(64):eabi8800.
544 26. Kono M, Saito S, Rokugo M, Egloff AM, and Uppaluri R. Enhanced oral versus flank
545 lymph node T cell response parallels anti-PD1 efficacy in head and neck cancer. *Oral*
546 *Oncol.* 2024;152:106795.
547 27. Ghorani E, Swanton C, and Quezada SA. Cancer cell-intrinsic mechanisms driving
548 acquired immune tolerance. *Immunity.* 2023;56(10):2270-95.
549 28. DuPage M, Mazumdar C, Schmidt LM, Cheung AF, and Jacks T. Expression of tumour-
550 specific antigens underlies cancer immunoediting. *Nature.* 2012;482(7385):405-9.
551 29. Probst HC, Lagnel J, Kollias G, and van den Broek M. Inducible transgenic mice reveal
552 resting dendritic cells as potent inducers of CD8+ T cell tolerance. *Immunity.*
553 2003;18(5):713-20.

30. Malhotra D, Linehan JL, Dileepan T, Lee YJ, Purtha WE, Lu JV, et al. Tolerance is established in polyclonal CD4(+) T cells by distinct mechanisms, according to self-peptide expression patterns. *Nat Immunol.* 2016;17(2):187-95.
31. Fitzgerald B, Connolly KA, Cui C, Fagerberg E, Mariuzza DL, Hornick NI, et al. A mouse model for the study of anti-tumor T cell responses in Kras-driven lung adenocarcinoma. *Cell Rep Methods.* 2021;1(5).
32. Damo M, Fitzgerald B, Lu Y, Nader M, William I, Cheung JF, et al. Inducible de novo expression of neoantigens in tumor cells and mice. *Nat Biotechnol.* 2021;39(1):64-73.
33. Dreno B, Thompson JF, Smithers BM, Santinami M, Jouary T, Gutzmer R, et al. MAGE-A3 immunotherapeutic as adjuvant therapy for patients with resected, MAGE-A3-positive, stage III melanoma (DERMA): a double-blind, randomised, placebo-controlled, phase 3 trial. *Lancet Oncol.* 2018;19(7):916-29.
34. Kjeldsen JW, Lorentzen CL, Martinenaite E, Ellebaek E, Donia M, Holmstroem RB, et al. A phase 1/2 trial of an immune-modulatory vaccine against IDO/PD-L1 in combination with nivolumab in metastatic melanoma. *Nat Med.* 2021;27(12):2212-23.
35. Pant S, Wainberg ZA, Weekes CD, Furqan M, Kasi PM, Devoe CE, et al. Lymph-node-targeted, mKRAS-specific amphiphile vaccine in pancreatic and colorectal cancer: the phase 1 AMPLIFY-201 trial. *Nat Med.* 2024;30(2):531-42.
36. Dolton G, Rius C, Wall A, Szomolay B, Bianchi V, Galloway SAE, et al. Targeting of multiple tumor-associated antigens by individual T cell receptors during successful cancer immunotherapy. *Cell.* 2023;186(16):3333-49.e27.
37. ElTanbouly MA, and Noelle RJ. Rethinking peripheral T cell tolerance: checkpoints across a T cell's journey. *Nat Rev Immunol.* 2021;21(4):257-67.
38. Damo M, Hornick NI, Venkat A, William I, Clulo K, Venkatesan S, et al. PD-1 maintains CD8 T cell tolerance towards cutaneous neoantigens. *Nature.* 2023;619(7968):151-9.
39. Yu J, Green MD, Li S, Sun Y, Journey SN, Choi JE, et al. Liver metastasis restrains immunotherapy efficacy via macrophage-mediated T cell elimination. *Nat Med.* 2021;27(1):152-64.
40. Nishimura H, Nose M, Hiai H, Minato N, and Honjo T. Development of lupus-like autoimmune diseases by disruption of the PD-1 gene encoding an ITIM motif-carrying immunoreceptor. *Immunity.* 1999;11(2):141-51.
41. Probst HC, McCoy K, Okazaki T, Honjo T, and van den Broek M. Resting dendritic cells induce peripheral CD8+ T cell tolerance through PD-1 and CTLA-4. *Nat Immunol.* 2005;6(3):280-6.
42. Ott PA, Hu-Lieskovan S, Chmielowski B, Govindan R, Naing A, Bhardwaj N, et al. A Phase Ib Trial of Personalized Neoantigen Therapy Plus Anti-PD-1 in Patients with Advanced Melanoma, Non-small Cell Lung Cancer, or Bladder Cancer. *Cell.* 2020;183(2):347-62 e24.

Figure1

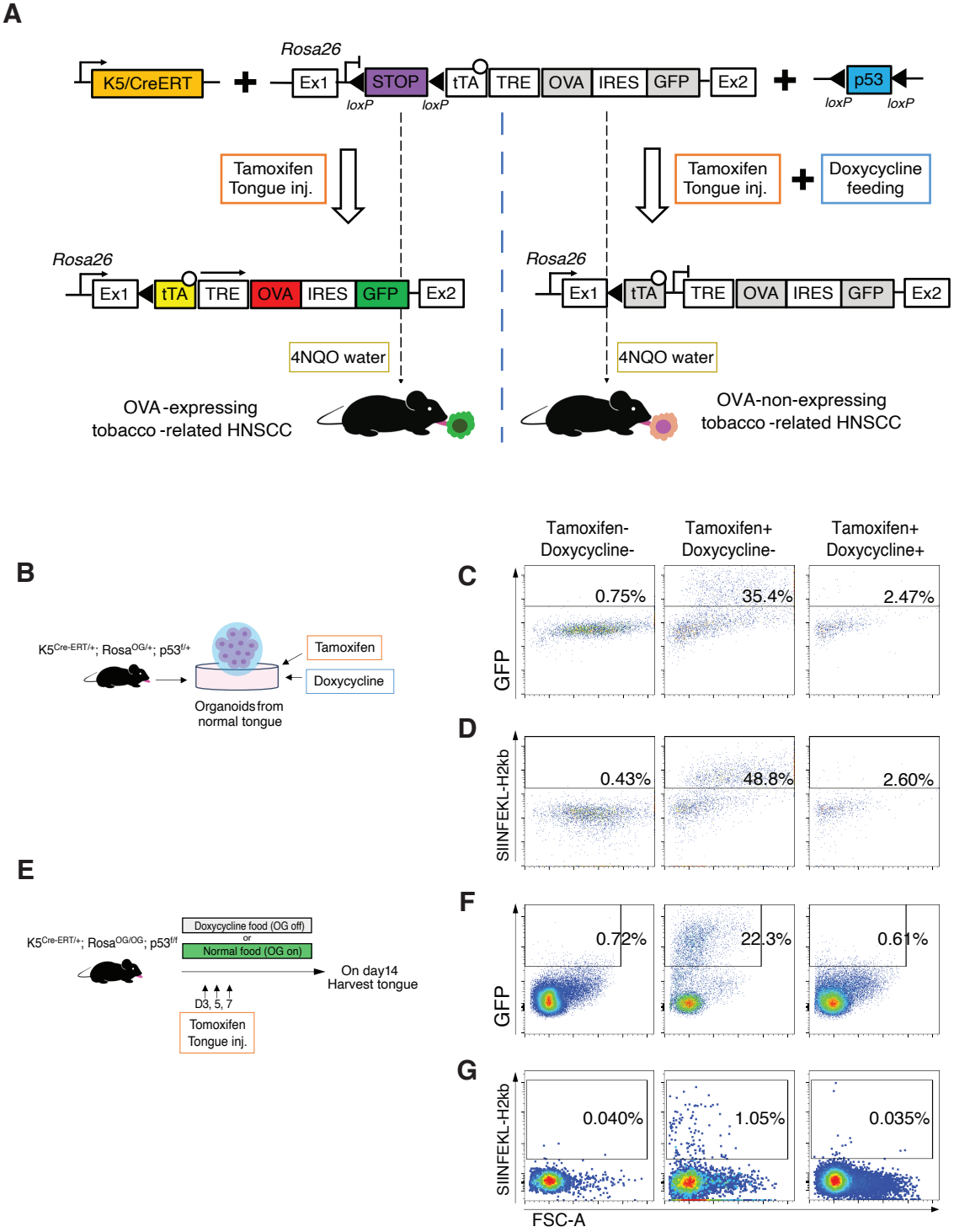
A
Rosa26
K5/CreERT
Ex1
STOP
tTA
TRE
OVA
IRES
GFP
Ex2
p53
loxP
loxP
loxP
loxP
Tamoxifen
Tongue inj.
Tamoxifen
Tongue inj.
Doxycycline
feeding
Rosa26
Ex1
tTA
TRE
OVA
IRES
GFP
Ex2
Rosa26
Ex1
tTA
TRE
OVA
IRES
GFP
Ex2
4NQO water
4NQO water
OVA-expressing
tobacco -related HNSCC
OVA-non-expressing
tobacco -related HNSCC
B
K5Cre-ERT/+; RosaOG/+; p53f/+
Tamoxifen
Doxycycline
Organoids from
normal tongue
E
K5Cre-ERT/+; RosaOG/OG; p53f/f
Doxycycline food (OG off)
or
Normal food (OG on)
On day14
Harvest tongue
D3, 5, 7
Tomoxifen
Tongue inj.
Tamoxifen-
Doxycycline-
Tamoxifen+
Doxycycline-
Tamoxifen+
Doxycycline+
C
GFP
0.75%
35.4%
2.47%
D
SIINFEKL-H2kb
0.43%
48.8%
2.60%
F
GFP
0.72%
22.3%
0.61%
G
SIINFEKL-H2kb
0.040%
1.05%
0.035%
FSC-A

600 **Figure 1: Establishment of KOG model**

601 A. Genetic loci and strategy for KOG model.

602 B. Experimental schema for C and D. Organoids were created from $K5^{Cre\text{-}ERT/+}$; $Rosa^{OVA\text{-}GFP(OG)/+}$;

603 $p53^{f/+}$ normal tongue and co-cultured with 4-hydroxytamoxifen (4-OHT, 2.5mM 96h) and then

604 with doxycycline (2μg/ml 48h). For H2kb-SIINFEKL staining, cells were pretreated with

605 100U/mL IFN-γ for 24h.

606 C and D. GFP expression (C) and SIINFEKL-H2kb expression (D) in KOG normal tongue

607 organoids treated with 4-OHT and doxycycline. Data were pre-gated on live and single cells.

608 Representative of 3 independent experiments.

609 E. Experimental schema for F and G. $K5^{Cre\text{-}ERT/+}$; $Rosa^{OG/OG}$; $p53^{f/f}$ mice were fed doxycycline or

610 normal food and 4-OHT was injected into the tongue epitheliums 3 times every 2 days and

611 harvested on day14.

612 F and G. GFP expression (F) and SIINFEKL-H2kb expression (G) in KOG mouse tongue treated

613 with 4-OHT and doxycycline. Data were pre-gated on live and single cells. Representative of 3

614 independent experiments.

615

616

617

618

619

620

621

Figure2

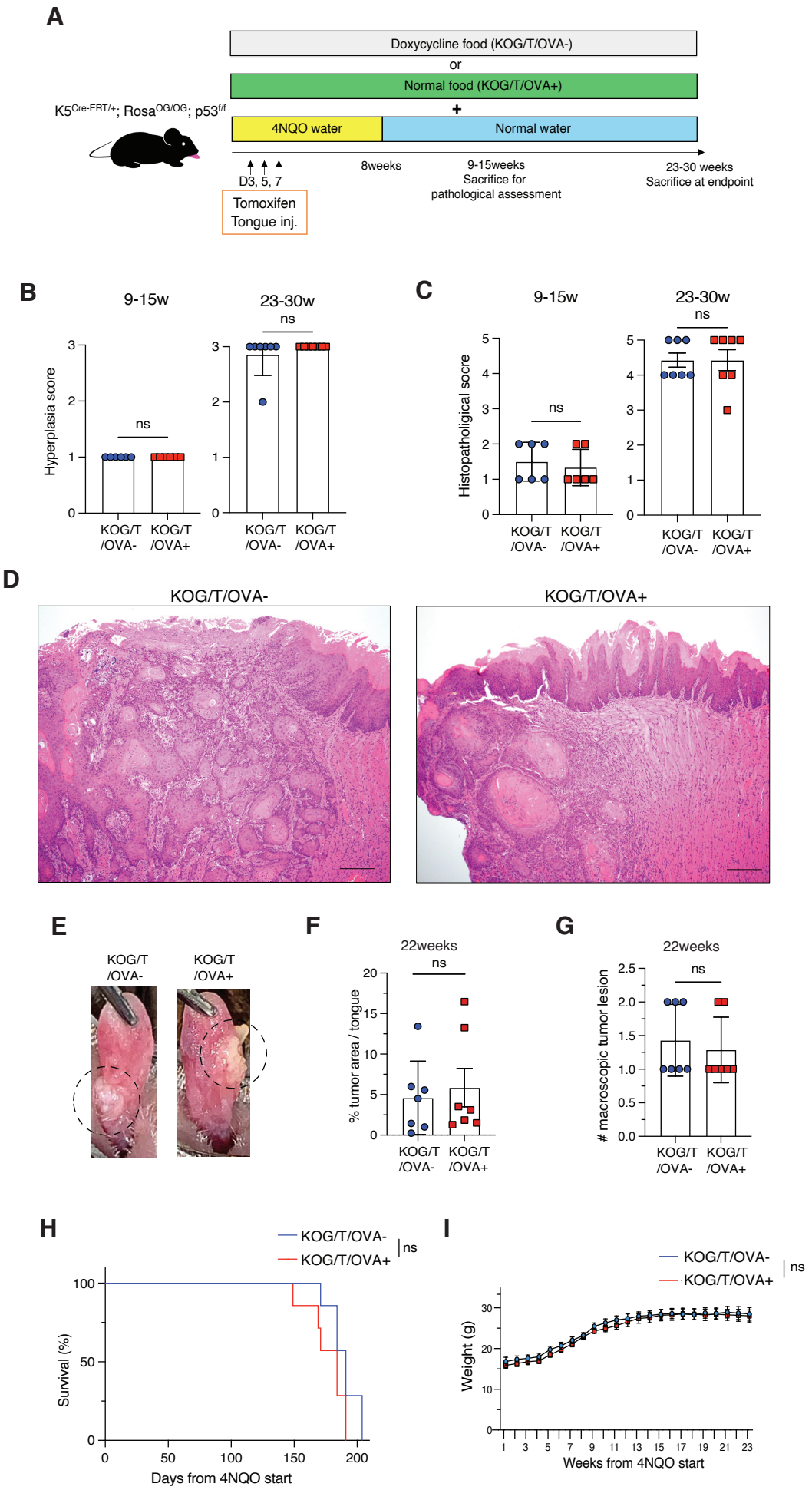
A
Doxycycline food (KOG/T/OVA-)
or
Normal food (KOG/T/OVA+)
+
K5Cre-ERT/+; RosaOG/OG; p53f/f
4NQO water
Normal water
D3, 5, 7
Tomoxifen
Tongue inj.
8weeks
9-15weeks
Sacrifice for
pathological assessment
23-30 weeks
Sacrifice at endpoint
B
9-15w
23-30w
ns
Hyperplasia score
KOG/T /OVA-
KOG/T /OVA+
C
Histopatholigical socre
D
KOG/T/OVA-
KOG/T/OVA+
E
F
22weeks
% tumor area / tongue
G
macroscopic tumor lesion
H
KOG/T/OVA-
KOG/T/OVA+
Survival (%)
Days from 4NQO start
I
Weight (g)
Weeks from 4NQO start

622 **Figure 2: Early expression of OVA antigen did not affect 4NQO-induced HNSCC**
623 **progression**

624 A. Experimental schema for B-H. KOG mice were provided with 4NQO water for 8 weeks and
625 then switched to normal water. Doxycycline or normal food was initiated concurrently with 4NQO.
626 4-OHT was injected on days 3, 5, and 7. Mice were sacrificed at specific time points or at the study
627 endpoint.

628 B. Epithelial hyperplasia scores on histopathological evaluation in KOG/T/OVA$^+$ and
629 KOG/T/OVA$^-$ mice at 9-15 weeks and 23-30 weeks (means ± SEM). The epithelial hyperplasia
630 score was categorized into four levels (0-3).

631 C. Histopathological scores in KOG/T/OVA$^+$ and KOG/T/OVA$^-$ at 9-15 weeks and 23-30 weeks
632 (means ± SEM). The histopathological scoring of the most severe lesion was categorized into six
633 levels: 0 for Normal, 1 for Atypia, 2 for Mild Dysplasia, 3 for Moderate Dysplasia, 4 for Severe
634 Dysplasia or Severe Papillary Dysplasia, and 5 for Squamous Cell Carcinoma (SCC).

635 D. Representative SCC lesion of tumor-bearing tongues of KOG/T/OVA$^+$ and KOG/T/OVA$^-$ mice
636 at 23-30 weeks.

637 E. Representative photographs of tumor-bearing tongues of KOG/T/OVA$^+$ and KOG/T/OVA$^-$
638 mice at 23-30 weeks.

639 F. Percentage of the macroscopic tumor area at 22 weeks (means ± SEM).

640 G. The number of the macroscopic tumor lesion at 22 weeks (means ± SEM).

641 H. Kaplan-Meier survival curve.

642 I. Weekly body weight.

643 *$p<0.05$, **$p<0.01$, ***$p<0.001$. Significance was evaluated by unpaired Student's t-test. Kaplan–
644 Meier curves were used for survival.

Figure3

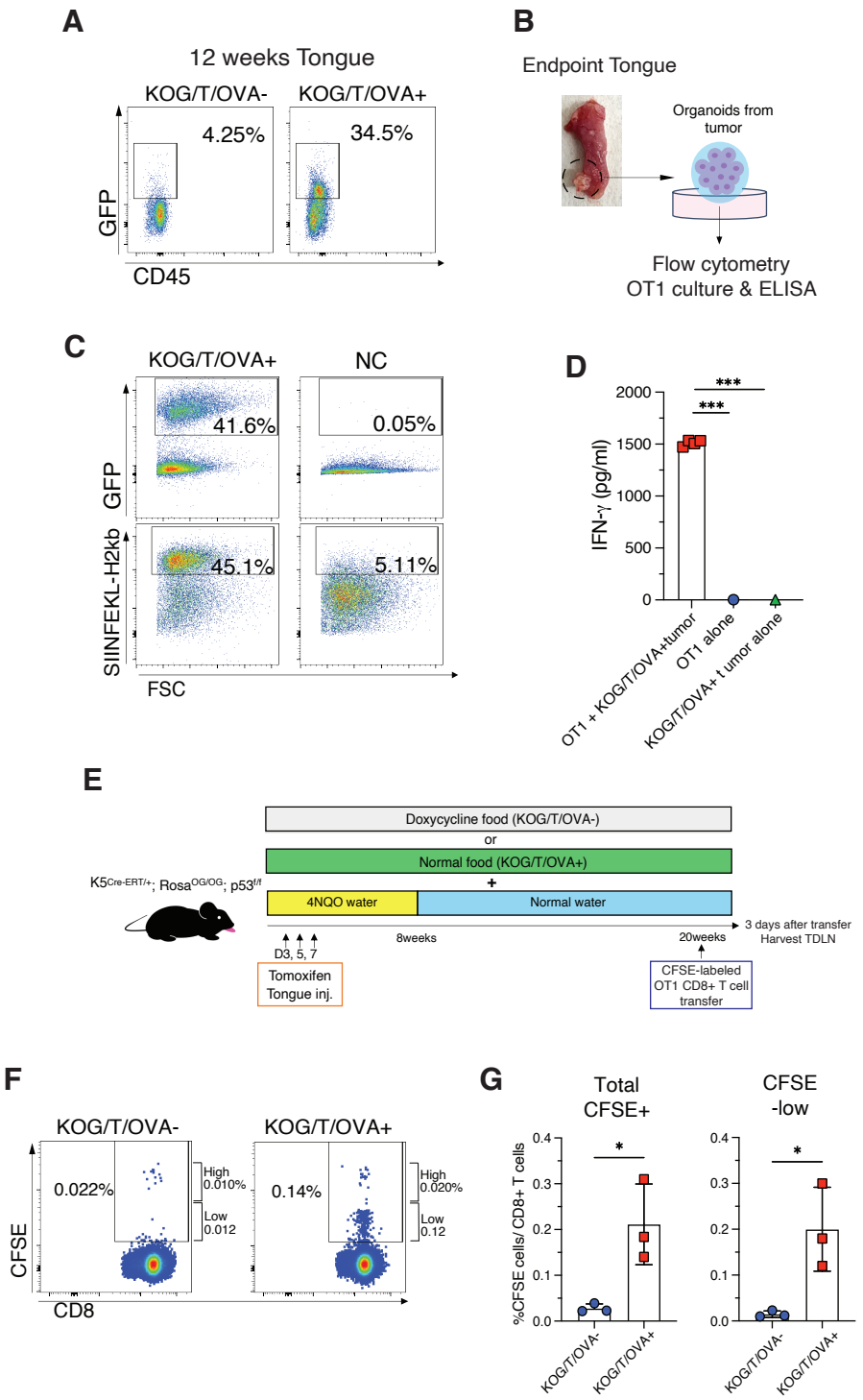
A
12 weeks Tongue
KOG/T/OVA-
KOG/T/OVA+
4.25%
34.5%
GFP
CD45
B
Endpoint Tongue
Organoids from tumor
Flow cytometry
OT1 culture & ELISA
C
KOG/T/OVA+
NC
41.6%
0.05%
45.1%
5.11%
GFP
SIINFEKL-H2kb
FSC
D
IFN-γ (pg/ml)
2000
1500
1000
500
0
***
***
OT1 + KOG/T/OVA+tumor
OT1 alone
KOG/T/OVA+ tumor alone
E
Doxycycline food (KOG/T/OVA-)
or
Normal food (KOG/T/OVA+)
+
4NQO water
Normal water
K5Cre-ERT/+; RosaOG/OG; p53f/f
D3, 5, 7
Tomoxifen
Tongue inj.
8weeks
20weeks
3 days after transfer
Harvest TDLN
CFSE-labeled
OT1 CD8+ T cell
transfer
F
KOG/T/OVA-
KOG/T/OVA+
0.022%
0.14%
High
0.010%
Low
0.012
High
0.020%
Low
0.12
CFSE
CD8
G
Total
CFSE+
CFSE
-low
%CFSE cells/ CD8+ T cells
0.4
0.3
0.2
0.1
0.0
*
*
KOG/T/OVA-
KOG/T/OVA+

645 **Figure 3: OVA expression was maintained on tumor cells during tumorigenesis**

646 A. GFP expression of the tongue epithelium cells from 12-weeks KOG/T/OVA$^+$ and KOG/T/OVA$^-$
647 mice. Data were pre-gated on live cells, single cells, and CD45-. Representative of three
648 independent experiments.

649 B. Experimental schema for C and D. Organoids were created from KOG/T/OVA$^+$ tongue tumors
650 and evaluated by flow cytometry and the experiment of OT-1 co-culture and ELISA experiments.

651 C. GFP and SIINFEKL-H2kb expression of the tumor organoids from tumor-bearing mouse
652 tongue. For assessment of SIINFEKL-H2kb expression, organoids were pre-treated with 100U
653 IFN-γ for 48h. Data were pre-gated on live and single cells. Representative of 3 independent
654 experiments.

655 D. Quantification of IFN-γ production in supernatants of the cultures with tumor cells and OT-1 T
656 cells (means ± SEM). Tumor organoids were dissociated into single cells and co-cultured with
657 OT-1 T cells for 24 hours. The supernatants were assessed by IFN-γ ELISA.

658 E. Experimental schema for F and G. CD8 T cells were purified from splenocytes of OT-1 mice
659 and labeled with CFSE. CFSE-labeled OT-1 CD8+ T cells were transferred into tumor-bearing
660 KOG mouse at 20 weeks and TDLNs were harvested 3 days after transfer.

661 F. CFSE expression in tumor draining lymph nodes (TDLNs) 3 days after OT-1 transfer. Data
662 were pre-gated on live cells, single cells, CD45+, CD3+, and CD8+ cells. CFSE-positive cells
663 were divided into CFSE-high (before or during differentiation) and -low cells (post-
664 differentiation). Representative of 2 independent experiments (n=3).

665 G. Quantification of the percentage of total of CFSE-positive, CFSE-high, and CFSE-low cells in
666 CD8+ T cells in TDLNs. Representative of 2 independent experiments (means ± SEM).

667 *$p<0.05$, **$p<0.01$, ***$p<0.001$. Significance was evaluated by unpaired Student's t-test.

Figure4

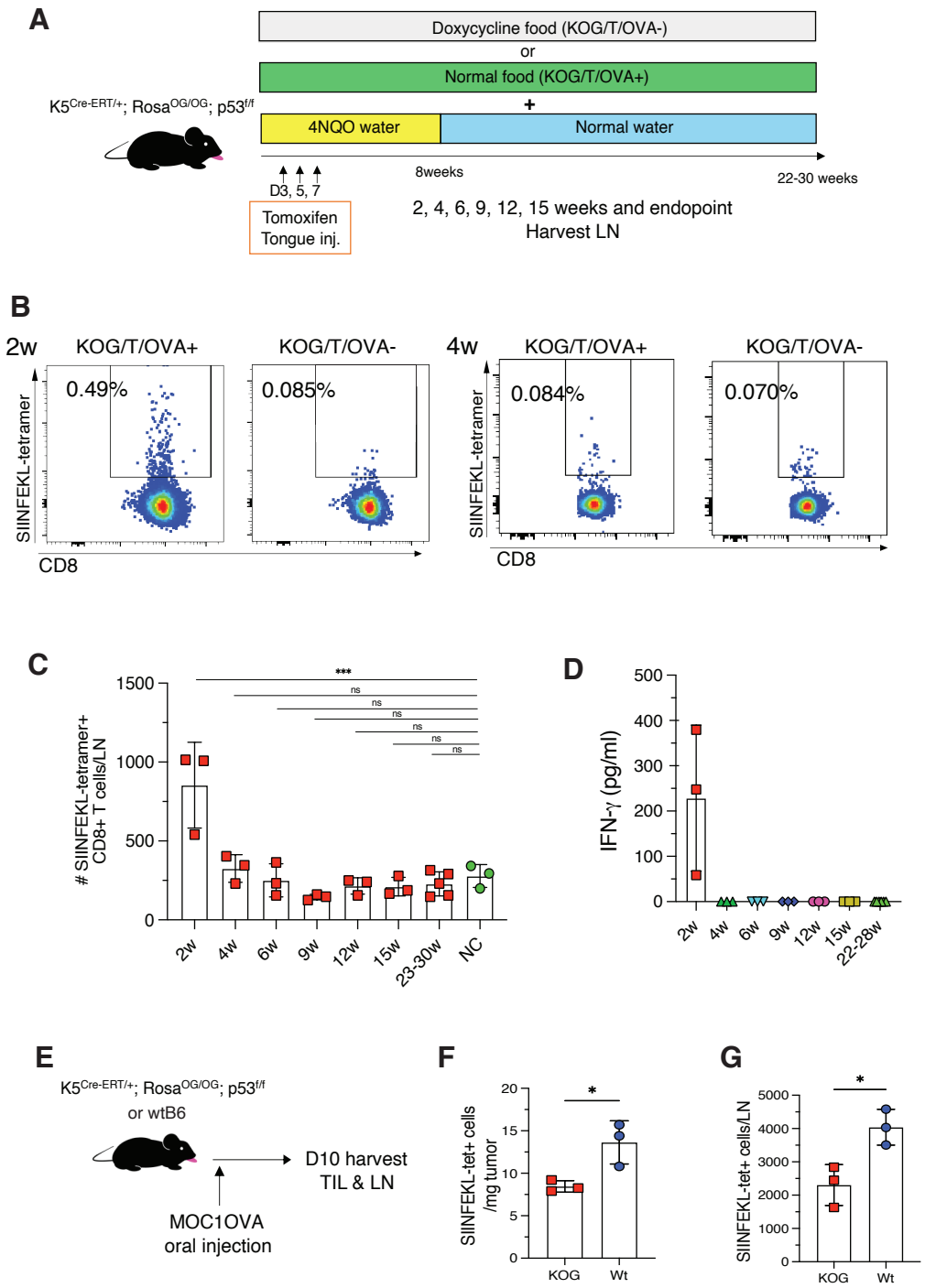
A
Doxycycline food (KOG/T/OVA-)
or
Normal food (KOG/T/OVA+)
+
K5Cre-ERT/+; RosaOG/OG; p53f/f
4NQO water
Normal water
8weeks
22-30 weeks
D3, 5, 7
Tomoxifen
Tongue inj.
2, 4, 6, 9, 12, 15 weeks and endopoint
Harvest LN
B
2w
KOG/T/OVA+
KOG/T/OVA-
4w
KOG/T/OVA+
KOG/T/OVA-
0.49%
0.085%
0.084%
0.070%
SIINFEKL-tetramer
CD8
C
SIINFEKL-tetramer+ CD8+ T cells/LN
1500
1000
500
0
***
ns
2w
4w
6w
9w
12w
15w
23-30w
NC
D
IFN-γ (pg/ml)
500
400
300
200
100
0
2w
4w
6w
9w
12w
15w
22-28w
E
K5Cre-ERT/+; RosaOG/OG; p53f/f
or wtB6
D10 harvest
TIL & LN
MOC1OVA
oral injection
F
SIINFEKL-tet+ cells /mg tumor
20
15
10
5
0
*
KOG
Wt
G
SIINFEKL-tet+ cells/LN
5000
4000
3000
2000
1000
0
*
KOG
Wt

668 **Figure 4: OVA-specific T cells were generated but subsequently became undetectable**

669 A. Experimental schema for B-D. KOG mice were treated with 4NQO, doxycycline, and 4-OHT
670 using the same protocol as in Figure 2A. Mice were sacrificed at specific time points or at the
671 study endpoint.

672 B. SIINFEKL-tetramer+ CD8+ T cells in DLNs from KOG/T/OVA^{+} mice 2 or 4 weeks after
673 treatment initiation. Data were pre-gated on live cells, single cells, CD45+, CD3+, and CD8+ cells.
674 LNs from doxycycline-treated mice were used as negative control of tetramer staining.
675 Representative of two independent experiments (n=3).

676 C. Quantification of the number of SIINFEKL-tetramer+ CD8+ T cells in DLNs from
677 KOG/T/OVA^{+} mice over the time course. Mice were sacrificed at each time point and DLNs were
678 analyzed. LNs from KOG/T/OVA^{-} were used as negative control of tetramer staining (NC).

679 D. Quantification of IFN-γ production in supernatants of the cultures with lymphocytes from
680 DLNs at each time points and SIINFEKL peptide (means ± SEM). DLNs were harvested at each
681 time point and isolated lymphocytes were co-cultured with SIINFEKL peptide for 24 hours. The
682 supernatants were assessed by IFN-γ ELISA.

683 E. Experimental schema for F and G. 3 million MOC1OVA cells were inoculated into left buccal
684 mucosa in KOG mice or wild type C57B/6 mice on day0. TILs and TDLNs were isolated on day10
685 and SIINFEKL-tetramer+ CD8+ T cells were analyzed by flow cytometry.

686 F and G. SIINFEKL-tetramer+ CD8+ T cells per mg tumor in TILs (F) or per LN in TDLNs (G).
687 *$p<0.05$, **$p<0.01$, ***$p<0.001$. Significance was evaluated by unpaired Student's t-test and
688 ANOVA with Tukey's multiple comparison adjustment.

689

690

Figure5

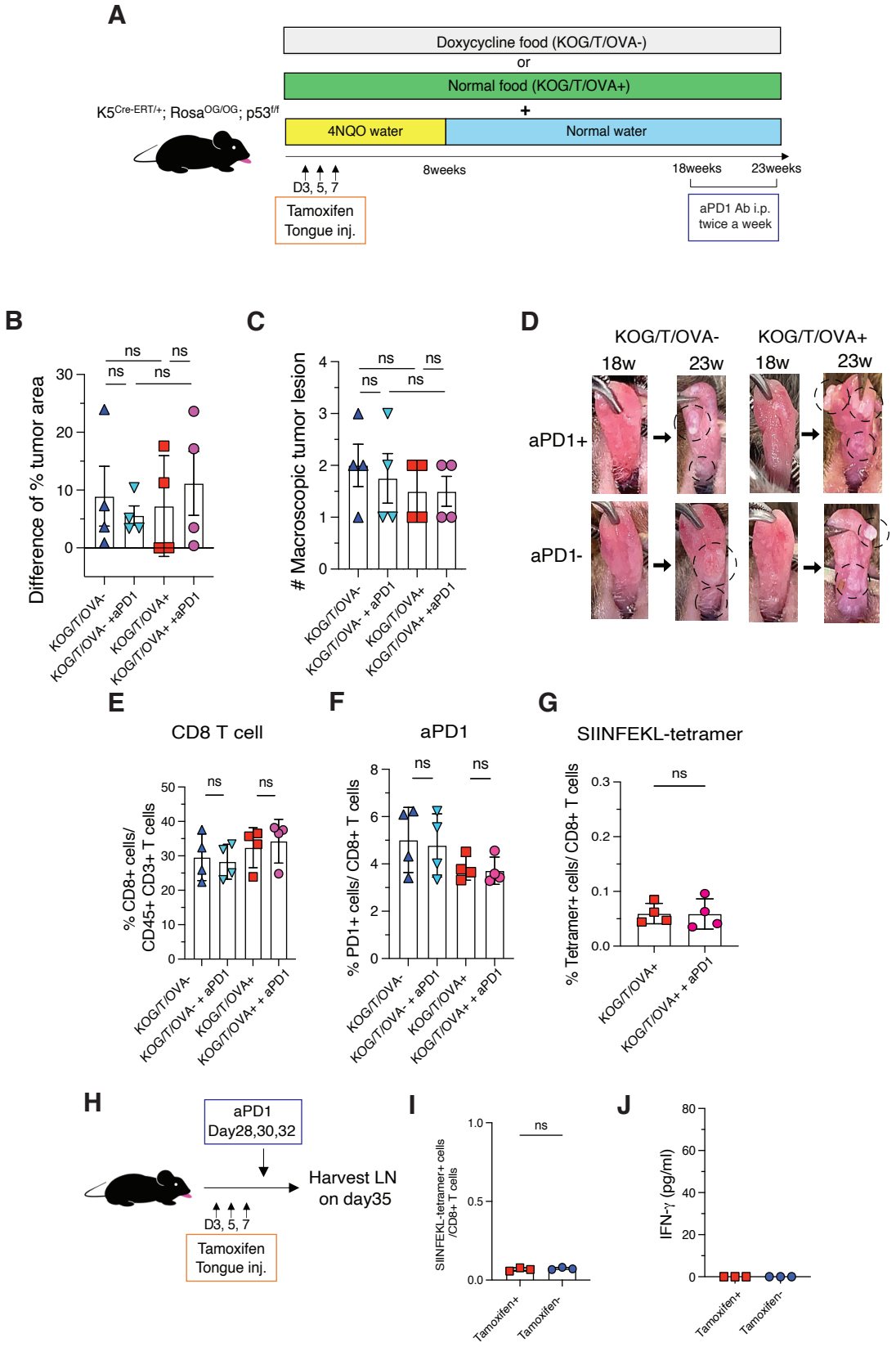
A
Doxycycline food (KOG/T/OVA-)
or
Normal food (KOG/T/OVA+)
+
K5Cre-ERT/+; RosaOG/OG; p53f/f
4NQO water
Normal water
8weeks
18weeks
23weeks
D3, 5, 7
Tamoxifen
Tongue inj.
aPD1 Ab i.p.
twice a week
B
Difference of % tumor area
ns
KOG/T/OVA-
KOG/T/OVA- +aPD1
KOG/T/OVA+
KOG/T/OVA+ +aPD1
C
Macroscopic tumor lesion
D
KOG/T/OVA-
KOG/T/OVA+
18w
23w
aPD1+
aPD1-
E
CD8 T cell
% CD8+ cells/
CD45+ CD3+ T cells
F
aPD1
% PD1+ cells/ CD8+ T cells
G
SIINFEKL-tetramer
% Tetramer+ cells/ CD8+ T cells
H
aPD1
Day28,30,32
Harvest LN
on day35
D3, 5, 7
Tamoxifen
Tongue inj.
I
SIINFEKL-tetramer+ cells
/CD8+ T cells
Tamoxifen+
Tamoxifen-
J
IFN-γ (pg/ml)

691 **Figure 5: aPD-1 blockade did not restore OVA-specific T cells and show no anti-tumor effect**

692 A. Experimental schema for the assessment of the anti-PD-1 anti-tumor effect. Treatment with
693 4NQO, doxycycline, and 4-OHT followed as in Figure 2A. anti-PD-1 Ab were injected twice a
694 week starting at 18 weeks and tongues were harvested at 23 weeks.

695 B. Difference in macroscopic tumor area before (18 weeks) and after (23 weeks) treatment (means
696 ± SEM).

697 C. The number of macroscopic tumor lesion at 23 weeks.

698 D. Photographs of KOG/T/OVA^{+} and KOG/T/OVA^{-} tongues before (18 weeks) and after (23
699 weeks) anti-PD-1 therapy.

700 E, F, G. The percentage of positive cells in TDLNs from 23 weeks tumor-bearing mice treated by
701 aPD-1 blockade (means ± SEM). E. CD8+ T cells in CD45+ CD3+ T cells. F. PD-1+ cells in CD8+
702 T cells. G. SIINFEKL-tetramer+ cells in CD8+ T cells.

703 H. Experimental schema for I and J. KOG mice were injected with 4-OHT on day3, 5, and 7 and
704 anti-PD-1 on day28, 30, and 32. DLNs were harvested on day35.

705 I. The percentage of SIINFEKL-tetramer+ cells in CD8+ T cells (means ± SEM).

706 J. Quantification of IFN-γ production in supernatants of the cultures with lymphocytes from DLNs
707 and SIINFEKL peptide (means ± SEM).

708 *$p<0.05$, **$p<0.01$, ***$p<0.001$. Significance was evaluated by unpaired Student's t-test and
709 ANOVA with Tukey's multiple comparison adjustment.

710

711

712

Figure6

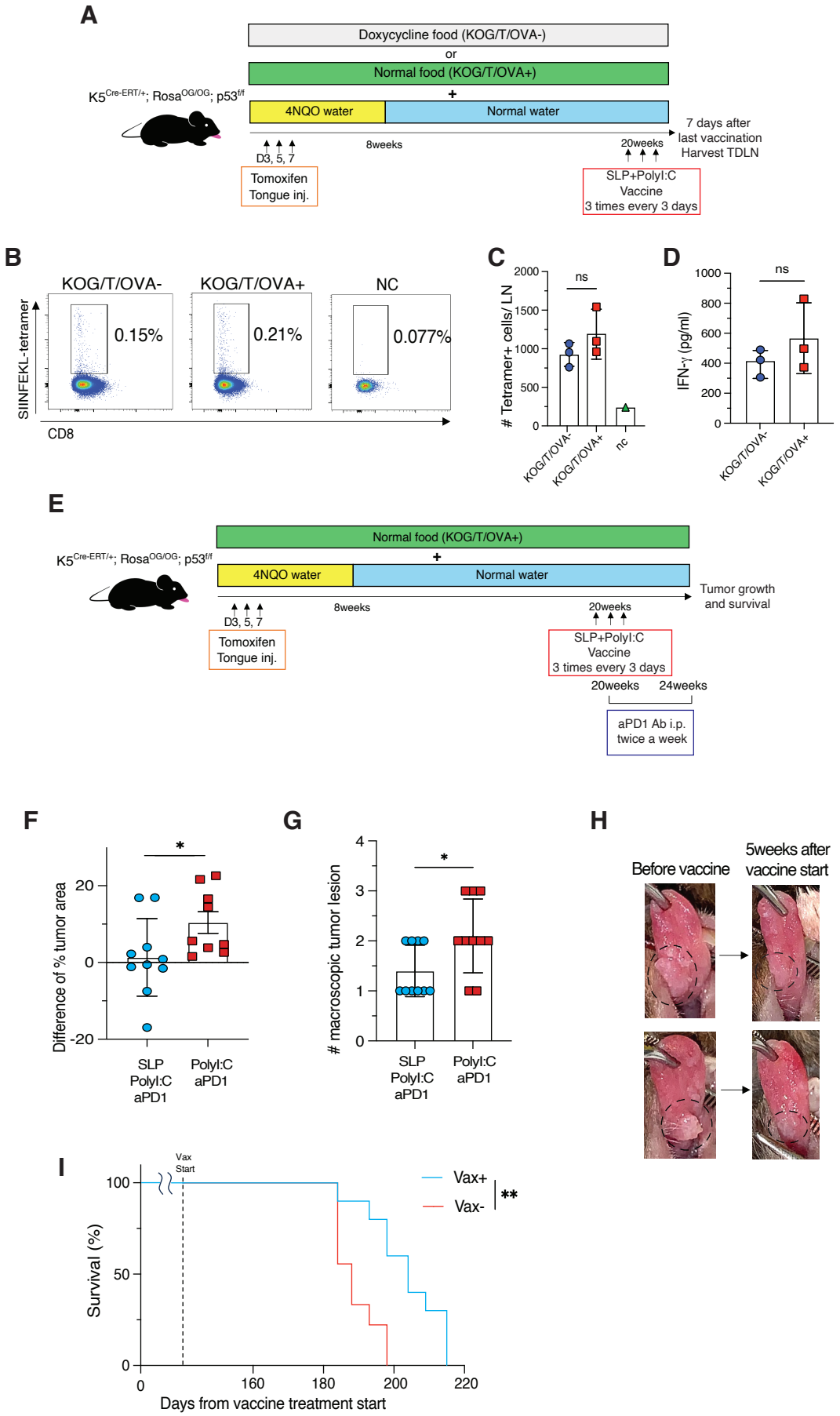
A
Doxycycline food (KOG/T/OVA-)
or
Normal food (KOG/T/OVA+)
+
4NQO water
Normal water
K5Cre-ERT/+; RosaOG/OG; p53f/f
D3, 5, 7
Tomoxifen
Tongue inj.
8weeks
20weeks
7 days after
last vaccination
Harvest TDLN
SLP+PolyI:C
Vaccine
3 times every 3 days
B
KOG/T/OVA-
KOG/T/OVA+
NC
0.15%
0.21%
0.077%
SIINFEKL-tetramer
CD8
C
Tetramer+ cells/ LN
ns
KOG/T/OVA-
KOG/T/OVA+
nc
D
IFN-γ (pg/ml)
ns
KOG/T/OVA-
KOG/T/OVA+
E
Normal food (KOG/T/OVA+)
+
4NQO water
Normal water
K5Cre-ERT/+; RosaOG/OG; p53f/f
D3, 5, 7
Tomoxifen
Tongue inj.
8weeks
20weeks
Tumor growth
and survival
SLP+PolyI:C
Vaccine
3 times every 3 days
20weeks
24weeks
aPD1 Ab i.p.
twice a week
F
Difference of % tumor area
*
SLP
PolyI:C
aPD1
PolyI:C
aPD1
G
macroscopic tumor lesion
*
SLP
PolyI:C
aPD1
PolyI:C
aPD1
H
Before vaccine
5weeks after
vaccine start
I
Vax
Start
Survival (%)
Vax+
Vax-
**
Days from vaccine treatment start

713 **Figure 6: Peptide vaccine restores OVA-specific T cells and attenuates tumor growth in**
714 **combination with anti-PD1**

715 A. Experimental schema for B-D. Treatment of 4NQO, doxycycline, and 4-OHT followed the
716 protocol in Figure 2A. 50μg OVA synthetic long peptide (SLP) containing SIINFEKL along with
717 100μg of polyI:C were injected into the buccal mucosa of tumor-bearing KOG mice three times
718 every three days, starting at 20 weeks. TLDNs were harvested 7 days after last vaccine.

719 B. SIINFEKL-tetramer+ CD8+ T cells in TDLNs from tumor-bearing KOG/T/OVA^{+} and
720 KOG/T/OVA^{-} mice . LNs from untreated KOG mice were used as negative control of tetramer
721 staining (NC). Representative of two independent experiments (n=3).

722 C. Quantification of the number of SIINFEKL-tetramer+ CD8+ T cells in TDLNs (means ± SEM).

723 D. Quantification of IFN-γ production in supernatants of the cultures with lymphocytes from
724 TDLNs and SIINFEKL peptide (means ± SEM). Isolated lymphocytes from TDLNs were co-
725 cultured with SIINFEKL peptide for 24 hours. Representative of two independent experiments.

726 E. Experimental schema for F-I. Treatment of 4NQO, doxycycline, 4-OHT, and vaccine followed
727 protocol outlined in Figure 6A. In addition, anti-PD-1 blockade was injected intraperitoneally
728 twice a week and continued for 5 weeks. Treatment with PolyI:C injection plus aPD-1 therapy was
729 used for control groups. F. Difference in macroscopic tumor area before (18 weeks) and after (23
730 weeks) treatment (means ± SEM).G. The number of macroscopic tumor lesion at 23 weeks. H.
731 Photographs of the KOG/T/OVA^{+} mouse tongues treated with vaccine and anti-PD-1 blockade. I.
732 Kaplan-Meier survival curve.

733 *$p<0.05$, **$p<0.01$, ***$p<0.001$. Significance was evaluated by unpaired Student's t-test and
734 ANOVA with Tukey's multiple comparison adjustment. Kaplan–Meier curve was used for
735 survival.